Analytical Sciences
Advance Publication by J-STAGE
Received July 3, 2018; Accepted July 27, 2018;
Published online on August 10, 2018
DOI: 10.2116/analsci.18P302

Original Papers

Nanostructured porous electrodes by the anodization of gold for application as scaffolds in direct-electron-transfer-type bioelectrocatalysis

Kento Sakai, Yuki Kitazumi, Osamu Shirai, and Kenji Kano†

* *Division of Applied Life Sciences, Graduate School of Agriculture, Kyoto University, Sakyo, Kyoto 606-8502, Japan*

† To whom correspondence should be addressed.

E-mail: kano.kenji.5z@kyoto-u.ac.jp (K. Kano)

Analytical Sciences
Advance Publication by J-STAGE
Received July 3, 2018; Accepted July 27, 2018;
Published online on August 10, 2018
DOI: 10.2116/analsci.18P302

Abstract

In this study, nanostructured porous gold electrodes were prepared by the anodization of gold in the presence of oxalic acid or glucose as a reductant and applied as scaffolds for direct electron transfer (DET)-type bioelectrocatalysis. Gold cation generated in the anodization seems to be reduced by the reductant to construct the porous gold structure. The DET-type performance of the electrode was examined using two DET-type model enzymes, bilirubin oxidase (BOD) and peroxidase (POD) for the four-electron reduction of dioxygen and the two-electron reduction of peroxide, respectively. BOD and POD on the anodized porous gold electrodes exhibited well-defined sigmoidal steady-state waves corresponding to DET-type bioelectrocatalysis. Scanning electron microscopy images revealed sponge-like pores on the electrodes. The anodized porous gold electrodes demonstrate promise as scaffolds for DET-type bioelectrocatalysis.

Keywords: Gold electrodes, anodization, reductant, direct-electron transfer, bioelectrocatalysis.

Analytical Sciences
Advance Publication by J-STAGE
Received July 3, 2018; Accepted July 27, 2018;
Published online on August 10, 2018
DOI: 10.2116/analsci.18P302

Introduction

Direct electron transfer (DET)-type bioelectrocatalysis involves the adsorption of enzymes on electrodes, which serve as catalysts for the electrolysis of substrates. This reaction combines an enzyme reaction with an electrode reaction.[1-7] Several bioelectrochemical devices can be efficiently constructed, e.g., biosensors, biofuel cells, and bioreactors. The rate constant for interfacial electron transfer in DET-type reactions exponentially decreases with increasing distance between the electrode surface and redox site of enzymes;[8-11] hence, it is crucial to minimize this distance and to control the orientation of enzymes on the electrodes.

In recent years, various electrode structures have been reported as scaffolds suitable for DET reactions.[1-7] For this purpose, carbon particles, carbon nanotubes,[12-27] and 3D gold nanostructures[28-34] have been frequently used because of the curvature effect of their structures to increases the probability of orientations suitable for DET reactions[26-27] and the facile surface functionalization with thiols as well as the high surface-to-volume ratios of the structures. However, it is difficult to precisely control the electrode shape of nanostructured materials. On the other hand, nanostructures have been reportedly prepared by the direct dealloying of bulk gold alloys.[35-39] However, it is difficult to prepare compositionally and crystallographically homogeneous alloys and to eliminate the complete contamination of alloying metals. In this regard, anodization is a simpler method, which is attractive for constructing porous structures on metal electrodes by the oxidation of the electrodes and reaction with the electrolyte under a positive electric field.[40] Thus far, the anodization of gold electrodes has been carried out in hydrochloric acid (HCl)- and organic acid-containing solutions.[41-44] For instance, the DET-type reaction of cytochrome P450 on an anodized gold electrode has been

Analytical Sciences
Advance Publication by J-STAGE
Received July 3, 2018; Accepted July 27, 2018;
Published online on August 10, 2018
DOI: 10.2116/analsci.18P302

reported.[44]

In this study, porous gold electrodes for DET-type bioelectrocatalysis were prepared by anodization in solutions containing oxalic acid or glucose as a reductant. Bilirubin oxidase (BOD) from *Myrothecium verrucaria* and peroxidase (POD) from horseradish were used as two model enzymes. BOD is a promising enzyme for the bioelectrocatalytic four-electron reduction of dioxygen (O_2) to water and is used as a catalyst for the cathode in various biofuel cells.[45] POD reduces hydrogen peroxide (H_2O_2) to water, and it is coupled with several oxidases to construct various bienzyme-type biosensors for the detection of the substrates of the oxidases. In the bienzyme-type biosensors, POD reaction is frequently coupled with electrode reactions using a mediator[46-50]. However, it has recently been reported that POD can work as a DET-type biocatalyst at suitable mesoporous electrodes to reduce H_2O_2 at a potential close to the redox potential of the protoheme (Compound I) of POD (0.7 V vs. Ag/AgCl at pH 7).[51-53] Such DET-type reactions of POD will draw attention of constructing bienzyme-type biosensors without any mediator. For practical purpose, it is important to easily construct scaffolds for DET-type enzymes. In this study, the morphology of the as-prepared porous gold electrodes and the characteristics of DET-type bioelectrocatalysis of BOD and POD on the electrodes were investigated.

Experimental

Chemicals

BOD (EC 1.3.3.5) from *M. verrucaria* was donated by Amano Enzyme Inc. (Japan), and POD (EC 1.11.1.7) from horseradish was purchased from Toyobo Co. (Japan); both enzymes were used without further purification. Oxalic acid was purchased from Nacalai Tesque, Inc. (Japan). Chloroauric acid ($HAuCl_4$) was obtained from Kishida Chemical Co., Ltd

Analytical Sciences
Advance Publication by J-STAGE
Received July 3, 2018; Accepted July 27, 2018;
Published online on August 10, 2018
DOI: 10.2116/analsci.18P302

(Japan). Other chemicals were purchased from Wako Pure Chemical Ind., Ltd. (Japan), and all solutions were prepared using distilled water.

Electrochemical measurements

All electrochemical measurements were conducted on an ALS 701E electrochemical analyzer. A Pt wire and a homemade Ag|AgCl|sat. KCl electrode were used as the counter and reference electrodes, respectively. All potentials described herein are expressed with respect to the reference electrode.

Electrode preparation

A gold electrode (99.95% purity, diameter 3.0 mm (projective surface area 0.071 cm^2), and length 25 mm, BAS) was polished using an alumina slurry with sizes of 3 and 0.5 μm, followed by sonication and washing with distilled water. The anodization of the gold electrode was carried out in the linear sweep voltammetry mode in a 0.3 M (M = mol dm^{-3}) oxalic acid solution at potentials ranging from 0.5 to 3.0 V under stirring at a scan rate (υ) of 0.1 mV s^{-1} and 0 °C with a cooling water circulation apparatus (EYELA, CA-3000, Japan). In addition, similar anodization was carried out in 1.0 M phosphate buffer (pH 7.0) containing 0.3 M glucose at potentials ranging from 0.5 V to 2.2 V under stirring at 0 °C and υ = 0.1 mV s^{-1}. After the anodization, the electrode surface was washed with 20 mM (for BOD) or 0.1 M (for POD) phosphate buffer (pH 7.0), respectively, and dried at room temperature. Then, a 30-μL aliquot of a 20 mg mL^{-1} (L = dm^3) BOD solution dissolved in 20 mM phosphate buffer (pH 7.0) was applied on the aforementioned electrodes, which were subsequently placed in a water-saturated atmosphere for 3 h at 4 °C for drying. A 20-μL aliquot of a 12 mg mL^{-1} POD solution dissolved in 0.1 M phosphate buffer (pH 7.0) containing 5% glutaraldehyde (GA) as a cross-linker reagent was applied on the aforementioned electrode surface and placed in a

Analytical Sciences
Advance Publication by J-STAGE
Received July 3, 2018; Accepted July 27, 2018;
Published online on August 10, 2018
DOI: 10.2116/analsci.18P302

water-saturated atmosphere for 2 h at 4 °C. GA was reported to improve the DET-type catalytic current density and stability of POD on mesoporous carbon electrodes.[51] The enzyme-modified electrodes were washed with a buffer solution before electrochemical measurements.

Spectroscopic observation of $HAuCl_4$ reduction

A 50 μL aliquot of a 0.1 mM $HAuCl_4$ solution was added to 450 μL of a 0.3 M oxalic acid solution or a 1.0 M phosphate buffer (pH 7.0) containing 0.3 M glucose at room temperature. The spectral change was measured using a Shimadzu UV-2550 UV-VIS spectrophotometer (Japan).

Microscopy measurements

Scanning electron microscopy (SEM) images were recorded on a Hitachi SU-8000 system (Hitachi High-Technologies, Japan). A thin porous gold foil was prepared by the anodization of a 10-μm gold foil (99.95% purity, Nilaco Corp., Japan) for SEM measurements, and the corresponding enzymes were immobilized on the anodized foil in a manner similar to that described in the section of *Electrode preparation*.

Results and Discussion

Characterization of the porous gold electrodes

The black line in Fig. 1(A) represents a linear sweep voltammogram (LSV) at a bare gold electrode in a 0.3 M oxalic acid solution under stirring. The current density at 3 V was 16 ± 3 mA cm^{-2} (note here that the errors in this study were evaluated using Student's *t* distribution at a 90% confidence level). After the anodization, the electrode surface changed to dark brown. Since oxalic acid is oxidized at potentials more positive than 1.2 V at a glassy carbon (GC)

Analytical Sciences
Advance Publication by J-STAGE
Received July 3, 2018; Accepted July 27, 2018;
Published online on August 10, 2018
DOI: 10.2116/analsci.18P302

electrode (Fig. S1(A)), the anodic current in Fig. 1(A) corresponds to the oxidation of oxalic acid and gold. The dark blown film was not produced in the absence of oxalic acid or without stirring even in the presence of oxalic acid. The SEM image of the porous gold foil anodized in solution (Fig. 1(B)) revealed that the electrode surface comprises sponge-like nanopores. The sponge-like structure is constructed by gold particles with a diameter of about 30 nm. There are large cavities and small gaps between gold particles in the structure.

In addition, similar anodization of gold in a phosphate buffer (pH 7.0) containing 0.3 M glucose as a reductant was observed (Fig. 1(A), gray line). The current density at 2.2 V was 3.5 ± 0.4 mA cm^{-2}. The electrode surface also became dark blown. Since glucose is not oxidized at a GC electrode (Fig. S1(B), the current is ascribed to the oxidation of gold in this case. The morphology of the electrode anodized in the glucose solution was slightly different (Fig. 1(C)) from that fabricated in the oxalic acid solution (Fig. 1(B)) as well as those fabricated in other organic acids reported previously.[42] The structure seems to be constructed by the aggregated gold nanoparticles with diameter of about 20 nm. The electrode surface also has large cavities and small gaps between gold particles. In the absence of the reductants, the electrode surface simply changed to orange and such porous structures were not observed after the electrolysis.

Some characteristics of anodization of gold have been reported previously.[41-44] However, the precise mechanism for the formation of porous structures by the anodization of gold in an oxalic acid or glucose solution remains unclear, although carbonaceous passivation film formation has been suggested to play a significant role in the development of porous structures.[41] Meanwhile, the formation mechanism of the porous structures during anodization in an HCl solution has been reported to be the combination of electrodissolution, disproportion, and deposition.[43]

Gold electrode surface is electrochemically oxidized to generate gold cations (Au^{3+} and Au^{+}).[54,55] We supposed that porous gold structures were constructed by the reduction of the

Analytical Sciences
Advance Publication by J-STAGE
Received July 3, 2018; Accepted July 27, 2018;
Published online on August 10, 2018
DOI: 10.2116/analsci.18P302

gold cations by oxalate ion or glucose as the reductant, because the presence of the reductant and the sufficient supply to the electrode for electrochemically active oxalate were crucial for constructing such porous structures by the anodization of gold. In order to verify the reduction, a model reaction was carried out using $AuCl_4^-$. On the addition of an oxalic acid solution to an $HAuCl_4$ solution, $AuCl_4^-$ was immediately reduced and no $[AuCl_4]^-$ remained in the solution after the reduction (Fig. 2(A)) The inside wall of a plastic vessel was gold-plated (Fig. 2(B)). On the other hand, when glucose was used as the reductant, gold colloid was generated and the solution changed blue as scattering light (Fig. 2(A)). Although the generation of gold nanoparticles are reported by the reduction of $[AuCl_4]^-$ in the presence of a stabilizer such as hexadecyltrimethylammonium bromide,[56] oxalate and glucose do not generate gold ion complex and simply work as a reductant in our case. It has been also reported that reduction of Au_2O_3 existing on electrode surface by glucose produces porous structures.[57] As a result, reduction of gold cations (and Au_2O_3 if any) generated during the anodization is a key reaction to construct the porous cold structure. The structures depend on the type of reductants and probably the reductant concentration and electrolysis conditions.

The morphological observation suggests drastic increase in the surface area by the anodization. Actually, the non-faradaic current density evaluated by cyclic voltammetry increased by 2-order of magnitude by the anodization. However, evaluation of electrochemically-active surface area of gold electrodes by cyclic voltammetry of iodine-adsorbed gold electrodes[57] indicated only about 10 times increase in the area by the anodization as compared with the planar electrode (Fig. S2)[58]. The contradictory result seems to indicate that some parts of the nanopores are electrochemically inactive, due for example to carbonaceous passivation film.[41] More detailed characterization is required to clarify the mechanism and the nanostructure.

Analytical Sciences
Advance Publication by J-STAGE
Received July 3, 2018; Accepted July 27, 2018;
Published online on August 10, 2018
DOI: 10.2116/analsci.18P302

DET-type bioelectrocatalysis at BOD- and POD-adsorbed electrodes

BOD and POD were homogeneously adsorbed on the porous structures on gold anodized in the 0.3 M oxalic acid solution (Figs. 1(D) and (E)). According to X-ray crystallography, the dimensions of BOD[59] and POD[60] are approximated to spheres with diameters of 5 and 4 nm, respectively. The SEM images seem to display a film covered with the electrode surface and a uniform and regular dense distribution for the BOD and POD domains.

The solid line in Fig. 3(A) shows a rotating disk cyclic voltammogram (RDCV) at the BOD-adsorbed porous gold electrodes under O_2-saturated conditions at pH of 5.0, a temperature of 25 °C, and an electrode rotating speed (ω) of 4,000 rpm. The black solid line in Fig. 3(A) represents the result obtained for the BOD-adsorbed electrode fabricated in the oxalic acid solution. A typical sigmoidal-wave was observed for O_2 reduction under rotating electrode conditions, corresponding to the DET-type bioelectrocatalysis for the reduction of O_2 by BOD as has been reported previously.[45] The catalytic current density at 0.1 V (4.0 ± 0.2 mA cm^{-2}) was similar to that of a BOD-adsorbed Ketjen Black-modified electrode, which is one of the most powerful, high-performance mesoporous biocathodes.[61] The catalytic current density reached one-half of the diffusion-controlled current density at a rotating disk electrode (–8.4 mA cm^{-2} at ω = 4,000 rpm and 25 °C[61] Note that the diffusion-controlled current density under rotating conditions does not reflect roughness factor of electrodes because of overlapping of diffusion layer.). The half-wave potential was 0.53 V for the sigmoidal wave and is close to the redox potential of the (electron-accepting) T1 copper site of BOD (0.460 V at pH 7.0)[62] obtained spectroelectrochemically and slightly more negative than the redox potential of H_2O/O_2 redox couple (0.62 V at pH 7.0).[63] These results are indicative of the improved performance for the heterogeneous electron transfer kinetics of BOD and an increase in the suitable orientation of the BOD molecules to the DET reactions at the porous gold electrode.

The inset of Fig. 3(A) shows the non-catalytic waves of BOD obtained under

Analytical Sciences
Advance Publication by J-STAGE
Received July 3, 2018; Accepted July 27, 2018;
Published online on August 10, 2018
DOI: 10.2116/analsci.18P302

Ar-saturated conditions at pH 5.0 (gray solid line) and pH 7.0 (black solid line). The midpoint potentials were 0.62 V and 0.52 V at pH 5.0 and 7.0, respectively. The value at pH 7.0 is almost identical to the half-wave potential of the sigmoidal O_2 reduction wave and that reported for carbon-nanotube-modified electrodes (0.53 V at pH 7.0)[61]. Based on these results, the porous gold electrode can be used as a scaffold for achieving favorable orientations for the adsorbed BOD and rapid interfacial electron-transfer kinetics.

Here, the porous electrodes were also prepared by the anodic oxidation in the glucose solution and the performance was examined. The gray solid line in Fig. 3(A) shows an RDCV at the BOD-adsorbed porous gold electrode anodized in the glucose solution. A typical sigmoidal DET-type bioelectrocatalytic wave corresponding to the reduction of O_2 was observed. The limiting value for the catalytic current density at 0.1 V (4.0 ± 0.3 mA cm^{-2}) and the half-wave potential were practically identical with those obtained for the porous electrode anodized in the oxalic acid solution, indicating that the electrode anodized in the glucose solution can also be used as a scaffold for the DET-type bioelectrocatalysis of BOD.

It is noteworthy that BOD adsorbed on a planar gold electrode showed only small catalytic wave with so-called residual slope and the half-wave potential was very negative (0.4 V) (Fig. S3(A)) The characteristics indicate random orientation of the enzyme with poor kinetics in the heterogeneous electron transfer. The anodization increased the catalytic current density by 3-order of magnitude (but the non-faradaic current density by 2-order of magnitude). The drastic improvement of the catalytic performance at the sponge-like anodized electrode is not simply ascribed to the increased surface area. We consider that the main factor corresponds to the curvature effect of the mesoporous structures, which increases in the probability of the orientations productive to DET-reaction, as evidenced theoretically.[29,30] The another conceivable reason is the intensified electric field in the diffuse double layer at the peak of nanostructured porous structures (presumably microporous structures); the electric field was intensified at the

Analytical Sciences
Advance Publication by J-STAGE
Received July 3, 2018; Accepted July 27, 2018;
Published online on August 10, 2018
DOI: 10.2116/analsci.18P302

peak of these structures because of the expansion of the diffuse double layers.[64] Heterogeneous electron transfer kinetics must be improved in such intensified electric field. Since the sponge-like anodized electrode can be used for a scaffold of DET-type reaction, it becomes important to clarify the dependence of the pore size and morphology on the performance of the DET-type bioelectrocatalysis in future.

Fig. 3(B) shows RDCVs at the POD-immobilized porous gold electrodes in 0.1 M phosphate buffer (pH 7.0) containing 0.2 mM H_2O_2. Non-catalytic signal of POD was not detected in the absence of H_2O_2. Typical sigmoidal waves were observed under rotating electrode conditions (ω = 4,000 rpm) for the electrodes anodized in the oxalic acid and glucose solutions, corresponding to the DET-type bioelectrocatalysis for the reduction of H_2O_2 with POD as has been reported previously.[51,52] The limiting current densities were 0.29 ± 0.05 mA cm^{-2} and 0.28 ± 0.04 mA cm^{-2} at the electrodes anodized in the oxalic acid and glucose solutions, respectively. POD modified on a planar gold electrode did not produce catalytic H_2O_2-reduction wave (Fig. S3(B)). The difference between the planar and porous electrodes is ascribed principally to the curvature effects of the mesoporous structures. The catalytic center of POD is a protoheme at which H_2O_2 is reduced to water in the presence of suitable electron donors and the ferric state of POD is oxidized to Compound I by H_2O_2 in a one-step two-electron reaction mechanism:

$$POD(Fe^{3+}) + H_2O_2 \rightarrow \text{Compound I} + H_2O \quad (1)$$

Compound I is re-reduced to the ferric state via Compound II as an intermediate:

$$\text{Compound I} + H^+ + e^- \rightarrow \text{Compound II} \quad (2)$$

$$\text{Compound II} + H^+ + e^- \rightarrow POD(Fe^{3+}) \quad (3)$$

The three redox states are reversible and the formal potential of the reactions given by Eqs. (2) and (3) were spectroelectrochemically determined as 0.75 and 0.72 V at pH 7.0, respectively.[65] These values are more negative than the redox potential of H_2O_2/H_2O couple (1.17 V at pH

Analytical Sciences
Advance Publication by J-STAGE
Received July 3, 2018; Accepted July 27, 2018;
Published online on August 10, 2018
DOI: 10.2116/analsci.18P302

7.0).[63] On the other hand, the half-wave potential of the sigmoidal catalytic wave of the H_2O_2 reduction wave was approximately 0.55 V. The result indicates that fast electron transfer from the electrode to the protoheme must occur. Non-catalytic redox reaction and bioelectrocatalytic H_2O_2-reduction of POD were reported.[66] However, most of non-catalytic DET signals of POD were observed around –0.2 V, which is assigned to the redox reaction of Fe^{3+}/Fe^{2+} of the protoheme that has no relation to the catalytic redox cycle. In addition, most of catalytic waves of POD without mediator reported in the literature have half-wave potentials approximately 0.2 V and the current densities are very low.[66] The catalytic wave observed in this work is very similar to definitive DET-type catalytic waves of POD.[51,52] This means that porous gold electrodes are superior scaffolds for DET-type reaction of POD in terms of simplicity of the fabrication in constructing versatile biosensing system.

The porous electrode anodized in the oxalic acid solution exhibited better performance than that anodized in the glucose solution with respect to the limiting current and half-wave potential. The porous structure constructed by anodization in the glucose solution most likely can hold limited amounts of electrochemically effective POD.[51] Meanwhile, the half-wave potential for the sigmoidal catalytic waves observed at the POD-adsorbed electrodes was similar to that observed for the non-catalytic DET signal of POD.[51] In addition, the electrode can be used as a new scaffold for the DET-type bioelectrocatalysis of POD. Porous gold electrodes are frequently used for catalytic systems without enzymes for various reactions such as carbon monoxide oxidation, methanol oxidation, glucose oxidation, O_2 reduction.[56,67] However, the overpotential of O_2 reduction and H_2O_2 reduction at the anodized gold electrode without enzymes (Fig. S4) were drastically decreased by the use of BOD and POD. Such enzymes are essential as electrocatalysts to reduce the overpotential and to increase the catalytic current density.

Analytical Sciences
Advance Publication by J-STAGE
Received July 3, 2018; Accepted July 27, 2018;
Published online on August 10, 2018
DOI: 10.2116/analsci.18P302

Conclusions

In this study, nanostructured porous gold electrodes were successfully prepared in an oxalic acid- or glucose-containing solution, which can be further applied as new scaffolds for the DET-type bioelectrocatalysis of BOD and POD. Electrochemical measurement results revealed well defined-sigmoidal signals for the two enzymes, corresponding to the O_2 reduction and H_2O_2 reduction. SEM measurements indicated that the anodized gold electrode comprises sponge-like structures. As the porous gold electrode structure would be affected by the reductants and anodization conditions, the electrodes can be possibly tuned for other individual redox enzymes via the understanding of the mechanism for the construction of such porous gold structures using reductants. The anodized porous gold electrodes proposed herein can serve as another important candidate for scaffolds, e.g., mesoporous gold microelectrodes smaller than 100 μm, for DET-type biosensors.

Acknowledgements

This work was supported by Research Fellowships of Japan Society for the Promotion of Science for Young Scientists No.16J08220 (to K.S.). A part of this work was supported by Kyoto University Nano Technology Hub in “Nanotechnology Platform Project” sponsored by the Ministry of Education, Culture, Sports, Science and Technology (MEXT), Japan No. 12024046. The authors thank Amano Enzyme Inc. for kind gifts of BOD and Enago (www.enago.jp) for the English language review.

Supporting Information

The optional figures are available free of charge on the Web at http://www.jsac.or.jp/analsci/.

Analytical Sciences
Advance Publication by J-STAGE
Received July 3, 2018; Accepted July 27, 2018;
Published online on August 10, 2018
DOI: 10.2116/analsci.18P302

References

1. C. Léger and P. Bertrand, *Chem. Rev.*, **2008**, *108*, 2379.
2. L. Gorton, A. Lindgren, T. Larsson, F. D. Munteanu, T. Ruzgas, and I. Gazaryan, *Anal. Chim. Acta*, **1999**, *400*, 91.
3. S. C. Barton, J. Gallaway, and P. Atanassov, *Chem. Rev.*, **2004**, *104*, 4867.
4. M. J. Moehlenbrock and S. D. Minteer, *Chem. Soc. Rev.*, **2008**, *37*, 1188.
5. V. Fourmond and C. Léger, *Curr. Opin. Electrochem.*, **2017**, *1*, 110.
6. A. D. Poulpiquet, A. Ciaccafava, and E. Lojou, *Electrochim. Acta*, **2014**, *126*, 104.
7. I. Mazurenko, A. D. Poulpiquet, and E. Lojou, *Curr. Opin. Electrochem.*, **2017**, *5*, 74.
8. R. A. Marcus, *Angew. Chem. Int. Ed.* **1993**, *32*, 1111.
9. C. C. Moser, J. M. Keske, K. Warncke, R. S. Farid, and P. L. Dutton, *Nature*, **1992**, *355*, 796.
10. P. L. Dutton, C. C. Page, C. C. Moser, and X. Chen, *Nature*, **1999**, *402*, 47.
11. H. B. Gray and J. R. Winkler, *Proc. Natl. Acad. Sci. U. S. A.*, **2005**, *102*, 3534.
12. F. Tasca, M. N. Zafar, W. Harreither, G. Nöll, R. Ludwig, and L. Gorton, *Analyst*, **2011**, *136*, 2033.
13. A. Ciaccafava, A. D. Poulpiquet, V. Techer, M. T. Giudici-Orticoni, S. Tingry, C. Innocent, and E. Lojou, *Electrochem. Commun.*, **2012**, *23*, 25.
14. K. Schubert, G. Goebel, and F. Lisdat, *Electrochim. Acta*, **2009**, *54*, 3033.
15. M. C. Weigel, E. Tritscher, and F. Lisdat, *Electrochem. Commun.*, **2007**, *9*, 689.
16. Y. Miura, S. Tsujimura, S. Kurose, Y. Kamitaka, K. Kataoka, T. Sakurai, and K. Kano, *Fuel Cells*, **2009**, *9*, 70.
17. S. Shleev, A. Jarosz-Wilkolazka, A. Khalunina, O. Morozova, A. Yaropolov, T. Ruzgas, and L. Gorton, *Bioelectrochemistry*, **2005**, *67*, 115.
18. K. So, Y. Kitazumi, O. Shirai, K. Nishikawa, Y. Higuchi, and K. Kano, *J. Mater. Chem. A*,

Analytical Sciences
Advance Publication by J-STAGE
Received July 3, 2018; Accepted July 27, 2018;
Published online on August 10, 2018
DOI: 10.2116/analsci.18P302

2016, *4*, 8742.

19. H. Funabashi, K. Murata, and S. Tsujimura, *Electrochemistry*, **2015**, *83*, 372.
20. S. Tsujimura, A. Nishina, Y. Hamano, K. Kano, and S. Shiraishi, *Electrochem. Commun.*, **2010**, *12*, 446.
21. K. Sakai, Y. Sugimoto, Y. Kitazumi, O. Shirai, K. Takagi, and K. Kano, *Electrochim. Acta*, **2017**, *228*, 537.
22. H. Xia, Y. Kitazumi, O. Shirai, H. Ozawa, M. Onizuka, T. Komukai, and K. Kano, *Bioelectrochemistry*, **2017**, *118*, 70.
23. A. Karimi, A. Othman, A. Uzunoglu, L. Stanciu, and S. Andreescu, *Nanoscale*, **2015**, *7*, 6909.
24. H. Funabashi, S. Takeuchi, and S. Tsujimura, *Sci. Rep.*, **2017**, *7*, 1.
25. S. Shleev, G. Shumakovich, O. Morozova, and A. Yaropolov, *Fuel Cells*, **2010**, *10*, 726.
26. Y. Sugimoto, Y. Kitazumi, O. Shirai, and K. Kano, *Electrochemistry*, **2017**, *85*, 8b2.
27. Y. Sugimoto, R. Takeuchi, Y. Kitazumi, O. Shirai, and K. Kano, *J. Phys. Chem. C*, **2016**, *120*, 26270.
28. X. Wang, M. Falk, R. Ortiz, H. Matsumura, J. Bobacka, R. Ludwig, M. Bergelin, L. Gorton, and S. Shleev, *Biosens. Bioelectron.*, **2012**, *31*, 219.
29. K. Murata, M. Suzuki, K. Kajiya, N. Nakamura, and H. Ohno, *Electrochem. Commun.*, **2009**, *11*, 668.
30. H. Matsumura, R. Ortiz, R. Ludwig, K. Igarashi, M. Samejima, and L. Gorton, *Langmuir*, **2012**, *28*, 10925.
31. K. Monsalve, M. Roger, C. Gutierrez-Sanchez, M. Ilbert, S. Nitsche, D. Byrne-Kodjabachian, V. Marchi, and E. Lojou, *Bioelectrochemistry*, **2015**, *106*, 47.
32. M. Pita, C. Gutierrez-Sanchez, M. D. Toscano, S. Shleev, and A. L. D. Lacey, *Bioelectrochemistry*, **2013**, *94*, 69.

Analytical Sciences
Advance Publication by J-STAGE
Received July 3, 2018; Accepted July 27, 2018;
Published online on August 10, 2018
DOI: 10.2116/analsci.18P302

33. K. Murata, K. Kajiya, N. Nakamura, and H. Ohno, *Energy Environ. Sci.* **2009**, *2*, 1280.
34. K. Sakai, Y. Kitazumi, O. Shirai, K. Takagi, and K. Kano, *Electrochem. Commun.*, **2017**, 84 75.
35. F. Jia, C. Yu, Z. Ai, and L. Zhang, *Chem. Mater.*, **2007**, *19*, 3648.
36. A. Castro-Muñiz, Y. Hoshikawa, H. Komiyama, W. Nakayama, T. Itoh, and T. Kyotani, *Front. Mater*., **2016**, *3*, 3.
37. H. Qiu, C. Xu, X. Huang, Y. Ding, Y. Qu, and P. Gao, *J. Phys. Chem. C*. **2008**, *112*, 14781.
38. X. Xiao, P. Si, and E. Magner, *Bioelectrochemistry*, **2016**, *109*, 117.
39. U. Salaj-Kosla, S. Pöller, Y. Beyl, M.D. Scanlon, S. Beloshapkin, S. Shleev, W. Schuhmann, and E. Magner, *Electrochem. Commun.*, **2012**, *16*, 92.
40. H. Masuda and K. Fukuda, *Science*, **1995**, *268*, 1466.
41. K. Nishio and H. Masuda, *Angew. Chem. Int. Ed*. **2011**, *50*, 1603.
42. K. Nishio and H. Masuda, *Bull. Chem. Soc. Jpn.*, **2013**, *86*, 1144.
43. Y. Deng, W. Huang, X. Chen, and Z. Li, *Electrochem. Commun.*, **2008**, *10*, 810.
44. Y. Mie, M. Ikegami, and Y. Komatsu, *Chem. Lett.* **2016**, *45*, 640.
45. N. Mano and A.D. Poulpiquet, *Chem. Rev.*, **2018**, *118*, 2392.
46. B. Bóka, N. Adányi, J. Szamos, D. Virág, and A. Kiss, *Enzyme Microb. Technol.* **2012**, *51*, 258.
47. C. H. Nieh, Y. Kitazumi, O. Shirai, and K. Kano, *Biosens. Bioelectron.* **2013**, *47*, 350.
48. R. Matsumoto, M. Mochizuki, K. Kano, and T. Ikeda, *Anal. Chem.* **2002**, *74*, 3297.
49. C.H. Nieh, S. Tsujimura, O. Shirai, and K. Kano, *Anal. Chim. Acta*, **2013**, *767*, 128.
50. J. Castillo, S. Gáspár, I. Sakharov, and E. Csöregi, *Biosens. Bioelectron.* **2013**, *18*, 705.
51. H. Xia, Y. Kitazumi, O. Shirai, and K. Kano, *Anal. Sci.*, **2017**, *33*, 839.
52. H. Xia, Y. Kitazumi, O. Shirai, H. Ohta, S. Kurihara, and K. Kano, *J. Electroanal. Chem.*, **2017**, *804*, 128.

Analytical Sciences
Advance Publication by J-STAGE
Received July 3, 2018; Accepted July 27, 2018;
Published online on August 10, 2018
DOI: 10.2116/analsci.18P302

53. Y. Okawa, N. Yokoyama, Y. Sakai, and F. Shiba, *Anal. Chem. Res.*, **2015**, *5*, 1.

54. J. C. Hoogvliet, M. Dijksma, B. Kamp, and W. P. V. Bennekom, *Anal. Chem.*, **2000**, *72*, 2016.

55. S. H. Cadle and S. Bruckenstein, *Anal. Chem.*, **1974**, *46*, 16.

56. M. C. M. Daniel and D. Astruc, *Chem. Rev.*, **2004**, *104*, 293.

57. W. Zhao, J. J. Xu, C. G. Shi, and H. Y. Chen, *Electrochem. Commun.*, **2006**, *8*, 773.

58. J. F. Rodriguez, T. Mebrahtu, and M. P. Soriaga, *J. Electroanal. Chem.,* **1987**, *233*, 283.

59. J. A. Cracknell, T. P. McNamara, E. D. Lowe, and C. F. Blanford, *Dalton Trans.*, **2011**, *40*, 6668.

60. G. I. Berglund, G. H. Carlsson, A. T. Smith, H. Szöke, A. Henriksen, and J. Hajdu, *Nature,* **2002**, *417*, 463.

61. K. So, Y. Kitazumi, O. Shirai, and K. Kano, *J. Electroanal. Chem.*, **2016**, *783*, 316.

62. S. Tsujimura, A. Kuriyama, N. Fujieda, K. Kano, and T. Ikeda, *Anal. Biochem.,* **2005**, *337*, 325.

63. A. J. Bard and L. R. Faulkner, *"Electrochemical Methods: Fundamentals and Applications"*, **2001**, John Wiley and Sons, New York.

64. Y. Kitazumi, O. Shirai, M. Yamamoto, and K. Kano, *Electrochim. Acta*, **2013**, *112*, 171.

65. M. Torimura, M. Mochizuki, K. Kano, T. Ikeda, and T. Ueda, *Anal. Chem.*, **1998**, *70*, 4690.

66. A. K. Yagati, and J.-W. Choi, *Electroanalysis*, **2014**, *26*, 1259.

67. R. Zhang and H. Olin, *Materials*, **2014**, 7, 3834.

Analytical Sciences
Advance Publication by J-STAGE
Received July 3, 2018; Accepted July 27, 2018;
Published online on August 10, 2018
DOI: 10.2116/analsci.18P302

Figure Captions

Fig. 1. (A) LSVs of bare gold electrodes in a 0.3 M oxalic acid solution (black line) and 1.0 M phosphate buffer (pH 7.0) containing 0.3 M glucose (gray line) at 0 °C and υ = 0.1 mV s^{-1} under stirring. (B) Top-view SEM image of a gold foil anodized in a 0.3 M oxalic acid solution (C) Top-view SEM image of a gold foil anodized in 1.0 M phosphate buffer (pH 7.0) containing 0.3 M glucose. (D) Top-view SEM image of a BOD-adsorbed gold foil anodized in a 0.3 M oxalic acid aqueous solution. (E) Top-view SEM image of a POD-immobilized gold foil anodized in a 0.3 M oxalic acid aqueous solution. The scale bars in each panel show 100 nm.

Fig. 2. (A) Adsorption spectra of a 13 μM $HAuCl_4$ solution before reduction (dotted line), and after addition of 0.28 M oxalic acid (solid line) and 0.28 M glucose in 0.9 M phosphate buffer (pH 7.0) (dashed line). (B) Photographic image of gold plating on a plastic Eppendorf tube after reduction of an $HAuCl_4$ solution by oxalic acid.

Fig. 3. (A) RDCVs for the reduction of O_2 at the BOD-modified porous gold electrode anodized in a 0.3 M oxalic acid solution (black solid line) and 1.0 M phosphate buffer (pH 7.0) containing 0.3 M glucose (gray solid line). Measurements were conducted in 0.2 M citrate buffer (pH 5.0) under O_2-saturated conditions at 25 °C, ω = 4,000 rpm, and υ = 10 mV s^{-1}. Black dotted and gray dashed lines represent CVs under Ar-saturated and quiescent conditions, respectively. Inset shows CVs under Ar-saturated conditions in 0.2 M citrate buffer (pH 5.0, gray solid line) and 0.1 M phosphate buffer (pH 7.0, black solid line), respectively, at υ = 5 mV s^{-1}. (B) RDCVs for the reduction of H_2O_2 at the POD-modified porous gold electrode anodized in a 0.3 M oxalic acid solution (black solid line) and 1.0 M phosphate buffer (pH 7.0) containing 0.3 M glucose (gray solid line). Measurements were conducted in 0.1 M phosphate buffer (pH 7.0) containing

Analytical Sciences
Advance Publication by J-STAGE
Received July 3, 2018; Accepted July 27, 2018;
Published online on August 10, 2018
DOI: 10.2116/analsci.18P302

0.2 mM H_2O_2 under air-saturated conditions at 25 °C, ω = 4,000 rpm, and υ = 10 mV s^{-1}. Black dotted and gray dashed lines represent CVs in the absence of the substrate, respectively.

Analytical Sciences
Advance Publication by J-STAGE
Received July 3, 2018; Accepted July 27, 2018;
Published online on August 10, 2018
DOI: 10.2116/analsci.18P302

Figures

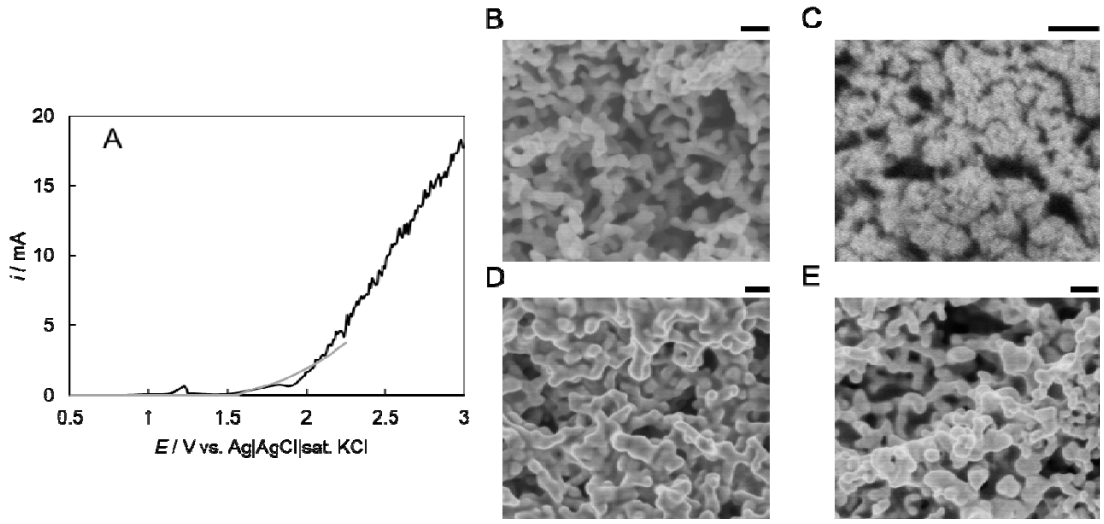

Fig. 1. (A) LSVs of bare gold electrodes in a 0.3 M oxalic acid solution (black line) and 1.0 M phosphate buffer (pH 7.0) containing 0.3 M glucose (gray line) at 0 °C and υ = 0.1 mV s^{-1} under stirring. (B) Top-view SEM image of a gold foil anodized in a 0.3 M oxalic acid solution (C) Top-view SEM image of a gold foil anodized in 1.0 M phosphate buffer (pH 7.0) containing 0.3 M glucose. (D) Top-view SEM image of a BOD-adsorbed gold foil anodized in a 0.3 M oxalic acid aqueous solution. (E) Top-view SEM image of a POD-immobilized gold foil anodized in a 0.3 M oxalic acid aqueous solution. The scale bars in each panel show 100 nm.

Analytical Sciences
Advance Publication by J-STAGE
Received July 3, 2018; Accepted July 27, 2018;
Published online on August 10, 2018
DOI: 10.2116/analsci.18P302

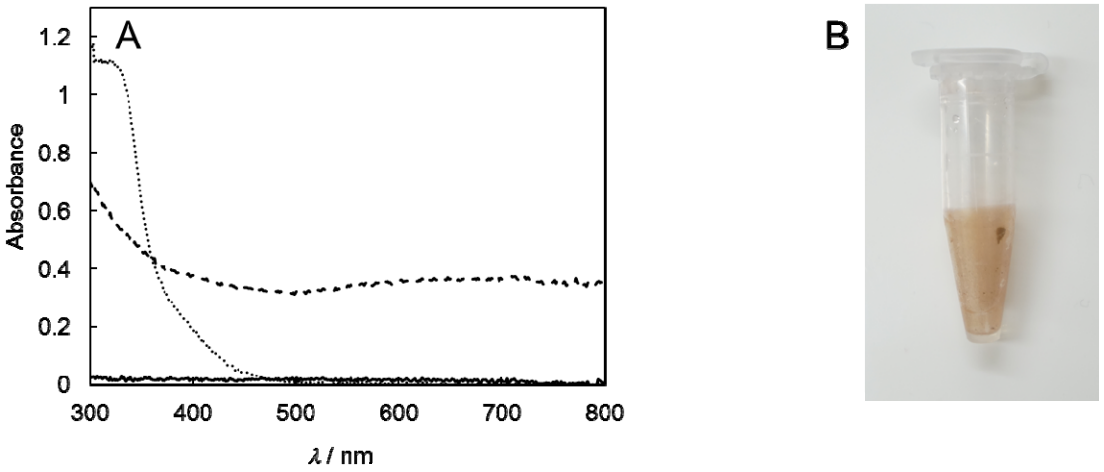

Fig. 2. (A) Adsorption spectra of a 13 μM $HAuCl_4$ solution before reduction (dotted line), and after addition of 0.28 M oxalic acid (solid line) and 0.28 M glucose in 0.9 M phosphate buffer (pH 7.0) (dashed line). (B) Photographic image of gold plating on a plastic Eppendorf tube after reduction of an $HAuCl_4$ solution by oxalic acid.

Analytical Sciences
Advance Publication by J-STAGE
Received July 3, 2018; Accepted July 27, 2018;
Published online on August 10, 2018
DOI: 10.2116/analsci.18P302

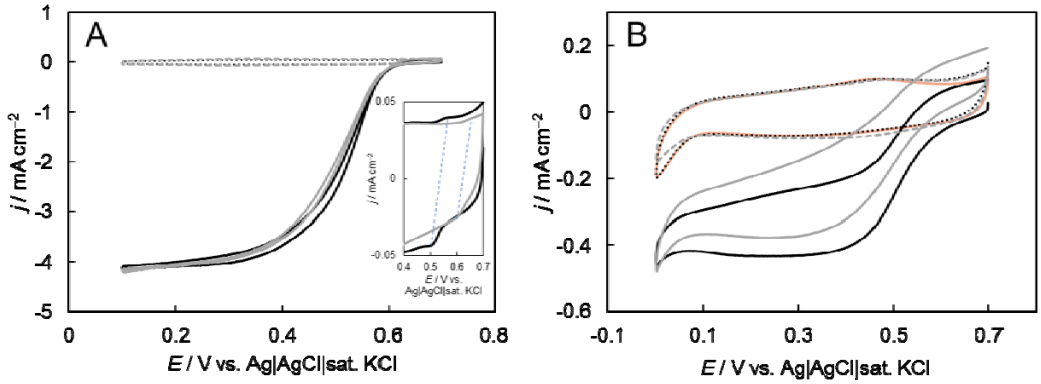

Fig. 3. (A) RDCVs for the reduction of O_2 at the BOD-modified porous gold electrode anodized in a 0.3 M oxalic acid solution (black solid line) and 1.0 M phosphate buffer (pH 7.0) containing 0.3 M glucose (gray solid line). Measurements were conducted in 0.2 M citrate buffer (pH 5.0) under O_2-saturated conditions at 25 °C, ω = 4,000 rpm, and υ = 10 mV s^{-1}. Black dotted and gray dashed lines represent CVs under Ar-saturated and quiescent conditions, respectively. Inset shows CVs under Ar-saturated conditions in 0.2 M citrate buffer (pH 5.0, gray solid line) and 0.1 M phosphate buffer (pH 7.0, black solid line), respectively, at υ = 5 mV s^{-1}. (B) RDCVs for the reduction of H_2O_2 at the POD-modified porous gold electrode anodized in a 0.3 M oxalic acid solution (black solid line) and 1.0 M phosphate buffer (pH 7.0) containing 0.3 M glucose (gray solid line). Measurements were conducted in 0.1 M phosphate buffer (pH 7.0) containing 0.2 mM H_2O_2 under air-saturated conditions at 25 °C, ω = 4,000 rpm, and υ = 10 mV s^{-1}. Black dotted and gray dashed lines represent CVs in the absence of the substrate, respectively.

Analytical Sciences
Advance Publication by J-STAGE
Received July 3, 2018; Accepted July 27, 2018;
Published online on August 10, 2018
DOI: 10.2116/analsci.18P302

Graphical Index